Journal of Materials Chemistry C

Accepted Manuscript

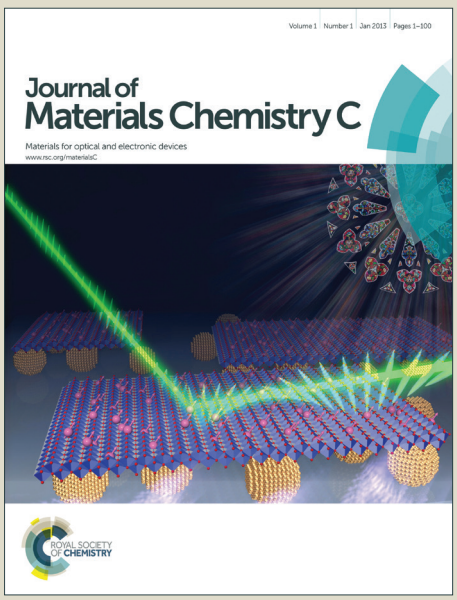

ROYAL SOCIETY OF CHEMISTRY

www.rsc.org/materialsC

Optoelectronic characteristics of near infrared light photodetector based on topological insulator Sb_2Te_3 film

*Kun Zheng,[1] Lin-Bao Luo,[1,]*Teng-Fei Zhang,[1] Yu-Hung Liu,[2, 3] Yong-Qiang Yu,[1] Rui Lu,[1] Huai-Li Qiu,[2] Zhong-Jun Li,[2] J. C. Andrew Huang[2 ,3,]**

[1] *School of Electronic Science and Applied Physics and Anhui Provincial Key Laboratory of Advanced Materials and Devices, Hefei University of Technology, Hefei, Anhui 230009, P. R. China*

[2] *Department of Physics, National Cheng Kung University, Tainan 701, Taiwan*

[3] *Taiwan Consortium of Emergent Crystalline Materials, Ministry of Science and Technology, Taipei 106, Taiwan*

* Corresponding author. E-mail: luolb@hfut.edu.cn (L. B. Luo), jcahuang@mail.ncku.edu.tw (J. C. A. Huang)

Acknowledgements

This work was supported by the Natural Science Foundation of China (NSFC, Nos. 61106010, 21101051), the Fundamental Research Funds for the Central Universities (2011HGZJ0004, 2012HGCX0003, 2013HGCH0012), and the Ministry of Science and Technology of Taiwan (NSC, 103-2923-M-006-001).

Introduction:

Topological insulator (e.g. Bi_2Se_3,[1] Bi_2Te_3,[2] and Sb_2Te_3[3]) is a bulk insulator with metallic surfaces. It is a kind of material characterized by a bulk band inversion and strong spin-orbit interaction which lead to surface states that bridge the bulk band gap. In the past decade, topological insulator have received substantial research attention owing to their exotic properties, and to date a number of synthetic methods such as pulsed-laser deposition (PLD),[4] chemical vapor deposition (CVD),[5] metal organic chemical vapor deposition (MOCVD),[6] and molecular beam epitaxy (MBE) have been developed to synthesize various topological insulators materials.[7, 8] It is reported that due to the spin-orbit coupling and time-reversal-symmetry,[2, 5, 9] there is low energy dissipation for the carriers on the surface states of topological insulators.[10, 11] What is more, angle-resolved photoemission spectroscopy (ARPES) analysis has observed that the surface states are composed of odd number of Dirac cones with helical spin-momentum textures.[12, 13] Topological insulator has exhibited great potential in a number of applications including quantum computing,[14, 15] spintronics,[16] thermoelectric devices,[4] photodetectors,[17, 18, 19] and superconductors.[20]

Of these devices with different functions photodetectors have received special research interest due to their wide-ranging application in many areas such as light vision, military surveillance, and target detection.[21, 22] For example, Zhang *et al.* has reported a new photodetector based on polycrystalline topological insulator Bi_2Te_3 film.[23] They found that the as-fabricated device exhibited obvious sensitivity to both visible and near infrared light (NIR) illumination with excellent reproducibility and stability. The responsivity and gain were estimated to be 3.3×10^{-5} A/W and 3.85×10^{-5} respectively. Moreover, Bao *et al* employed graphene-Bi_2Te_3 nano-heterojunction to fabricate photo-switches for detection of irradiation in the range from 532 to 1550 nm. It was

observed that the device had a very high responsivity of 10 AW^{-1}, and a photoconductive gain of 11.[24] Herein, we present a NIR photodetector based on topological insulator Sb_2Te_3 film grown by MBE. It was found that the NIR photodetector exhibits obvious sensitivity to the 980 nm light illumination at low temperature with excellent reproducibility. The responsivity, photoconductivity gain, and I_{on}/I_{off} were estimated to be 21.7 A/W, 27.4 and 2.36, respectively, which are much better than other topological insulator films based devices. This study suggests that topological insulator Sb_2Te_3 films have great potential for future opotoelectroinic devices application.

Results and Discussion

Figure 1(a) schematically illustrates the device geometry of the as-fabricated NIR photodetector, which is fabricated from topological insulator Sb_2Te_3 film with thickness of ~50 nm. From the XRD pattern of the film shown in **Figure 1(b)**, one can see clearly that all the diffraction peaks can be readily indexed to rhombohedral crystal structure with a space group number of R-3m(166) (JCPDS Card No.71-0393), consistent with literature value.[25] In addition, the growth orientation is along [00X] direction. The sharp streaky patterns of RHEED in the **Figure 1(c)** indicate that the topological insulator Sb_2Te_3 is of single crystal, which is different from the polycrystallinity of topological insulator synthesized by PLD.[23] According to the schematic illustration shown in **Figure 1(d)**, the crystal structure of Sb_2Te_3 actually consists of five-atom layers along *Z*-direction, which is known as quintuple layer. Each quintuple layer consists of five atoms with Te1-Sb-Te2-Sb'-Te1' (Te1 and Te1', Sb and Sb' are equilibrium, Te2 is third atom). ARPES measurement along the $\Gamma - K$ direction was then carried out to study the electronic band structure of the Sb_2Te_3 film. As shown in the **Figure 1(e)**, the white lines show the upper surface state band (SSB), and the blue lines

correspond to the bulk valence band (BVB). As a matter of fact, the topological insulator behavior of the Sb_2Te_3 film was also confirmed by the Dirac point slightly near the Fermi level around the Γ axis, which is consistent with theoretical calculation.[26]

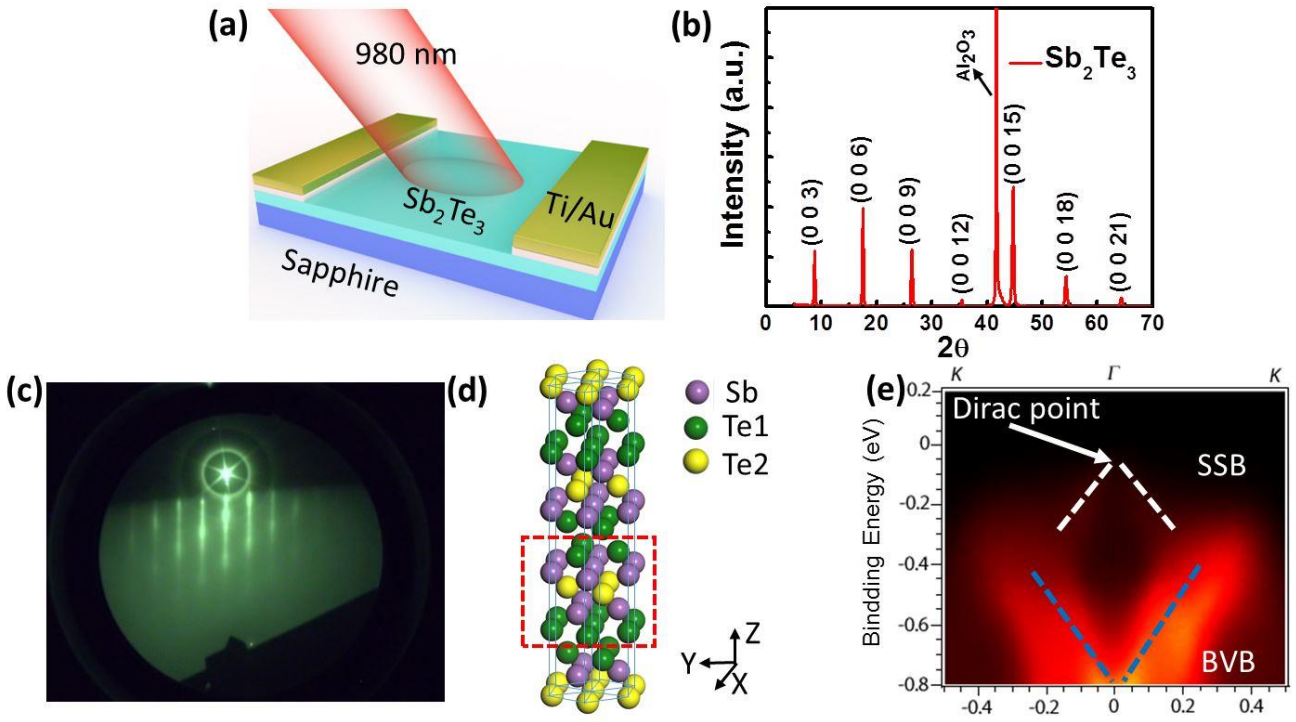

Figure 1 (a) The schematic illustration of NIR photodetector based on topological insulator Sb_2Te_3 film. (b) X-ray diffraction (XRD) pattern of the Sb_2Te_3 film that is grown at 250 °C by MBE. (c) RHEED pattern of Sb_2Te_3 film. (d) Schematic illustration of the crystal structure of the Sb_2Te_3 film. (e) ARPES intensity map as a function of binding energy and momentum.

The temperature-dependent current-voltage (*I*-*V*) curves of the topological insulator Sb_2Te_3 film was then studied in order to reveal its electrical characteristics. **Figure 2(**a) and (b) compare the *I*-*V* characteristics at varied temperatures ranging from 8.5 to 300 K in dark and under 980 nm light illumination (6.2 mW/cm^2). It is clear that the resistance in dark increases with decreasing temperature, which is attributed to the special electronic structure where Fermi level locates near the Dirac point. The *I*-*V* curves in dark situation exhibits weak non-linear behavior, which is due to the existence of barrier between the topological thin film and metal electrode. Interestingly, when

illuminated by 980 nm light, the *I-V* curves are virtually linear, signifying that good contact (Ohmic contact) was formed between the topological insulator film and Ti/Au electrode. It is also found that the dark-current increases with increasing temperature, in rough agreement with previous study.[27] In fact, similar phenomenon is also observed when the device is illuminated by 980 nm light. Notably, the currents under light illumination are all larger than that without illumination in the whole temperature region. From the temperature dependent resistances of the material at the bias of $V = 1$ V shown in **Figure 2(c)**, one can see that the resistance in dark is falling more quickly than that under 980 nm light illumination. To estimate the contact resistance, we compared the *I-V* characteristic at temperature of both 45 and 300 K using both two-probe methods [Figure 2(d)]. The contact resistance between the Sb_2Te_3 film and Ti/Au electrodes and the resistance of Sb_2Te_3 film were estimated by the formula of $2R_c+R_{4p}=R_{2p}$， where R_c is resistance of the contact resistance, R_{2p} and R_{4p} are the resistance measured by the two-probe and four-probe measurements, respectively. By fitting the linear part near the 0 V from -0.1 to 0.1 V, both the R_{2p} and R_{4p} at 45 K were calculated to be about 515.7 and 508.3 V respectively. In addition, the contact resistance at this temperature is about 7.4, which is 1.46% of the resistance of Sb_2Te_3 film. What is more, the contact resistance at 300 K is only 0.27% of the resistance of Sb_2Te_3 film. In light of the relatively small contact resistance, we used two-point method through the optoelectronic measurements for convenience.

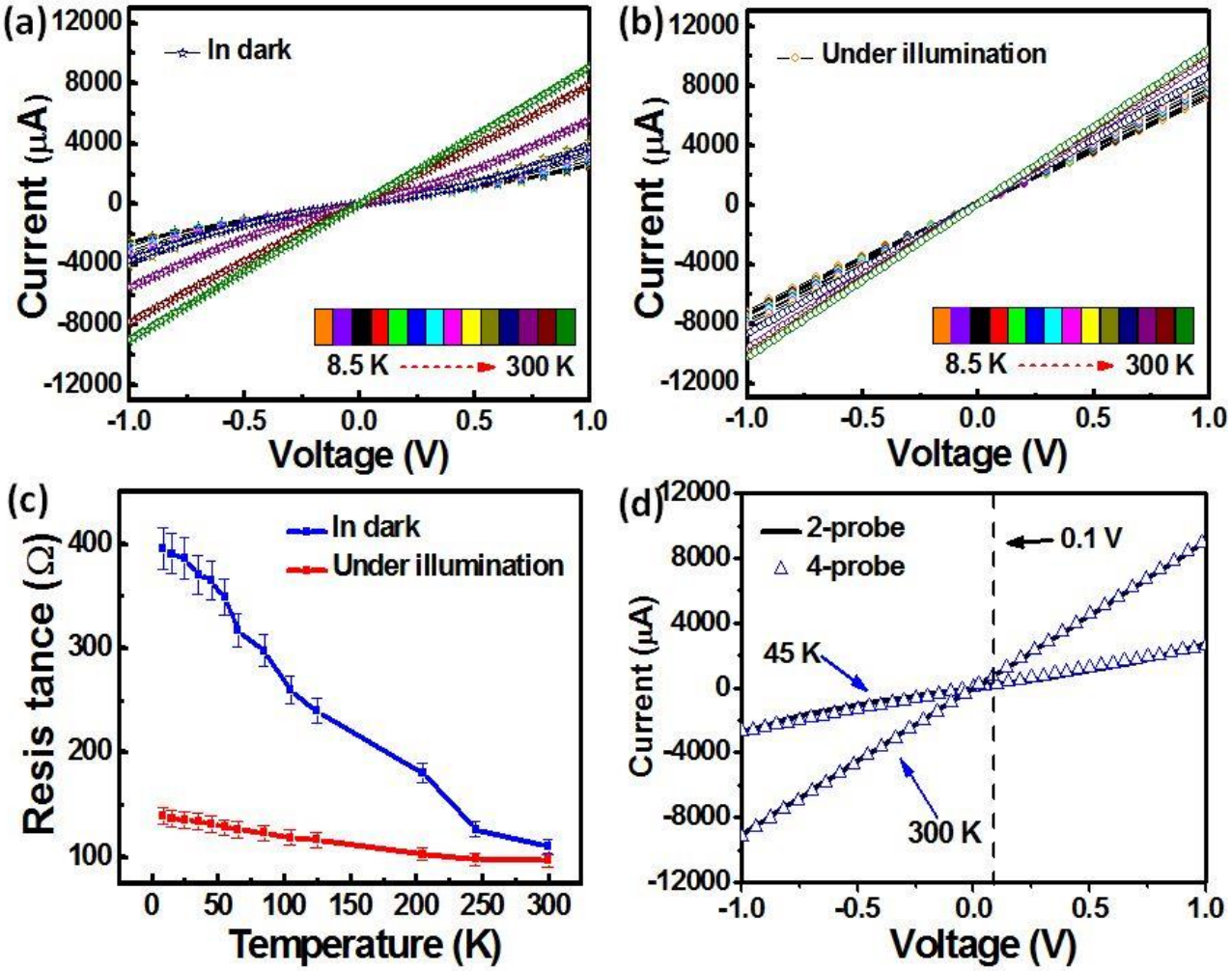

Figure 2 Typical I-V curves of the Sb_2Te_3 film in dark (a) and under illumination (b) at varied temperature from 8.5 to 300 K. (c) The comparison of the resistances in dark and under 980 nm light illumination at different temperature, the bias voltage is set to be 1 V. (d) The I-V characteristics of Sb_2Te_3 film by two- and four-probe measurements.

In light of the temperature-dependent electrical property of Sb_2Te_3 film, the photoresponse characteristics at different temperatures was then studied. As depicted in **Figure 3(a)**, the electrical current increases to a high-conduction "on" state when irradiated by 980 nm light, but it decreases to low-conductivity "off" state after the NIR illumination was switched off. Unlike the conventional photodetectors based on semiconductor nanostructure with very fast response speed,[28, 29] the present device has relatively slow rise time and fall time (~several hundred seconds). Such a difference in response speed is probably due to their distinction in working mechanism. In order to quantitatively evaluate the device performance of the NIR photodetector, the responsivity (R) and photoconductive

gain (G) of the device under different temperatures are calculated by the following formulas.[30, 31]

$$R = \frac{I_p - I_d}{P_{opt}} = \frac{\Delta I}{P_{opt}} = \eta\left(\frac{q\lambda}{hc}\right)G \quad (1)$$

$$G = R\frac{hc}{\eta q\lambda} \quad (2)$$

Where I_p, I_d, P_{opt}, η, q, λ, h and c are the photocurrent, the current without light illuminated on, the power of the light which is irradiated on the device, the quantum efficiency (for convenience, assuming η =1),[32] the absolute value of electron charge (1.6×10^{-19} Coulombs), the wavelength of illuminated light (980 nm), the Planck's constant (6.626×10^{-34} J s) and the velocity of light (3×10^{8} m/s), respectively. Based on the above equations, the responsivity of the device at the temperature from 8.5 to 165 K is keeping increasing and the maximum value is approaching 3.5 AW^{-1}. Then, the responsivity begins falling until 0.5 AW^{-1} at the temperature range from 165 to 300 K. Similar gain dependence on temperature was observed, as illustrated by the red curve in **Figure 3(b)**. The relatively high responsivity and gain at 150 K is related to the operation mechanism. As discussed later, the photocurrent of the present NIR photodetector was contributed by both the bulk and surface states, which exhibit different responsive behavior: the bulk state (Eg: 0.26 eV), like other semiconductor materials normally exhibit high responsivity at room temperature, while the surface state in contrast is good at detecting at low temperature. Such a difference in optoelectronic properties causes a relatively high responsivity and gain at moderate temperature.

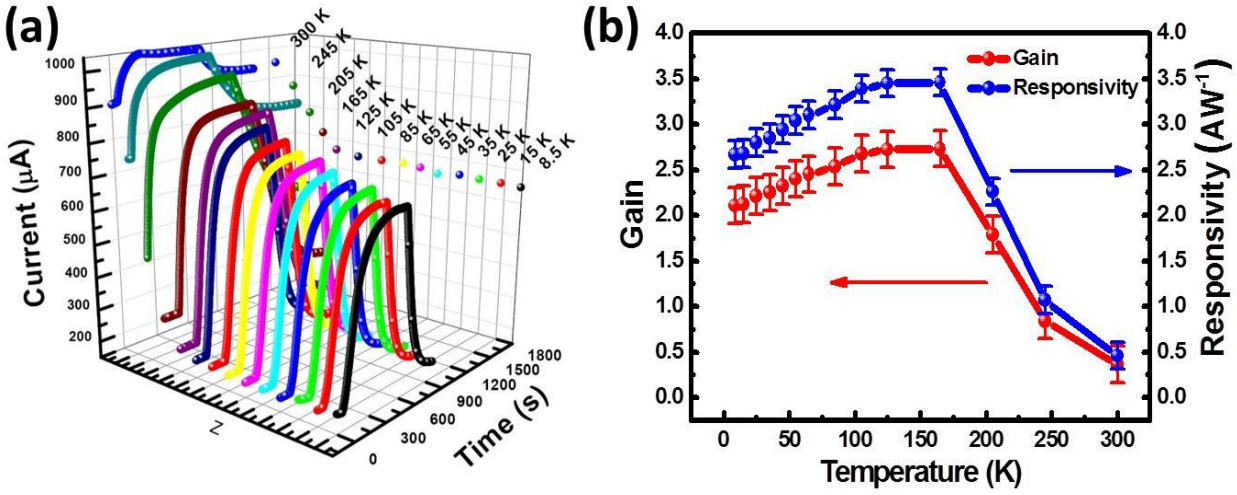

Figure 3 (a) Time response of the topological insulator Sb_2Te_3 film photodetector under 980 nm light irradiation at different temperatures and the bias is fixed at 0.1 V. (b) Responsivity and gain of the photodetector with various temperatures.

It is interesting to note that the photocurrent of the present NIR photodetector exhibits high dependence on the intensity of the incident irradiation as well. **Figure 4(a)** plots the photocurrent of Sb_2Te_3 photodetector under illumination with different power intensity ranging from 340 μW/cm^2 to 6.2 mW/cm^2. It is clear that the photocurrent of the device increases gradually with increasing light intensity. Further quantitative analysis of the relationship between the photocurrent and the light intensity find that the photocurrent can be fitted by simple power law: $I=AP^{\theta}$, where A is the constant for a certain wavelength, P is the varied intensity of the light which is illuminated on the device and θ is a constant that determines the photosensitivity of the photodetector.[33] Fitting the equation by the experimental data gives $\theta \approx 0.755$ (**Figure 4(b)**). Understandably, such a non-integer exponent can be regarded as a consequence of complex process of electron-hole generation, trapping and recombination with the topological insulator film upon NIR irradiation.[31]

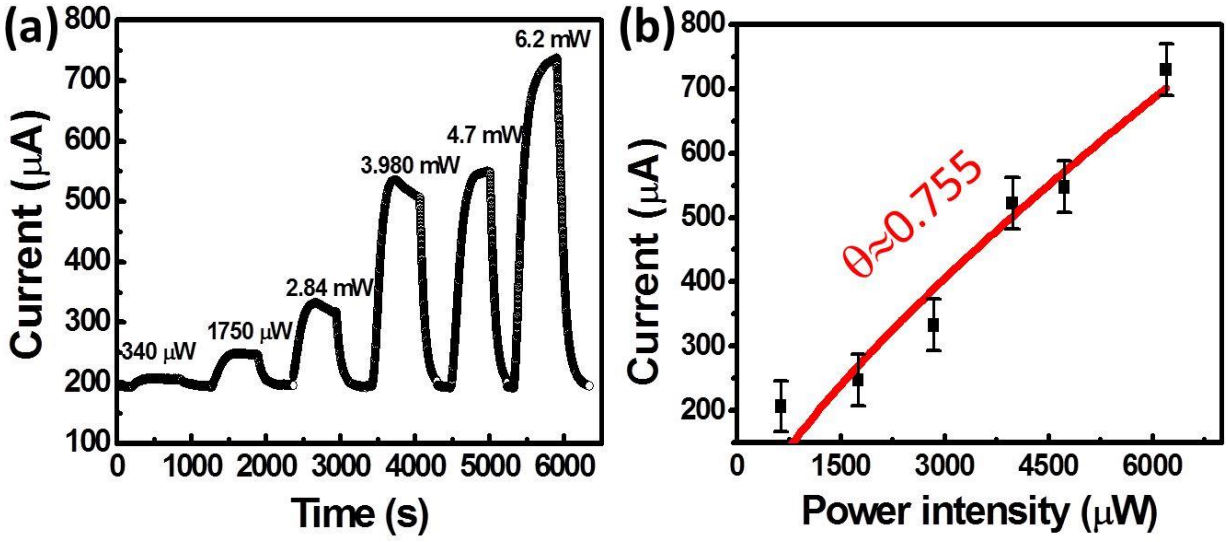

Figure 4 (a) the photocurrent of the device with different power 980 nm light illuminated from 86.5 μW/cm^2 to 6.2 mW/cm^2. (b) The relationship between the power intensity and the photocurrent.

In addition to light intensity, the photocurrent of our topological insulator device is dependent on bias voltage as well. **Figure 5(a)** plots the dark current, photocurrent and on/off ratio (I_{on}/I_{off}) as a function of different bias voltages, from which the currents in dark and under irradiation are observed to increase with increasing voltage at different rates, giving rise to slow decrease with increasing bias voltage. To further reveal the bias voltage-dependent optoelectronic property of the NIR photodetector, the photoresponse at bias voltage of 1, 0.1 and 0.01 V under NIR illumination that was periodically switched on and off is investigated. As shown in **Figure 5(b)**, at all 3 bias voltages, the present device displays obvious sensitivity to NIR illumination with good stability and reproducibility. The corresponding on/off ratios (I_{light}/I_{dark}) are estimated to be 2.36, 3.77 and 4.23 for 1, 0.1 and 0.01 V, respectively. Furthermore, by using the above Formula (1) and (2), the responsivity and photoconductive gain are estimated to be 21.7, 2.31, and 0.263 AW^{-1} and 27.4, 2.93 and 0.333, for 1, 0.1 and 0.01 V respectively. Based on these results, it can be concluded that both responsivity and gain of the device increase with increasing bias voltage. Besides, to determine how weak

irradiation could be distinguished from the noise, the specific detectivity (D^*) is calculated by the following equation[34, 35, 36]:

$$D^* = RS^{\frac{1}{2}} \Big/ \left(2qI_d\right)^{\frac{1}{2}} = \Delta I S^{\frac{1}{2}} \Big/ P_{opt}\left(2qI_d\right)^{\frac{1}{2}} \quad (3)$$

where R is the responsivity, S is the effective area between the parallel electrodes, q is the electronic charge, I_d is the dark current. By using the experimental data mentioned above, the detectivity is determined to be 1.22×10^{11}, 5.66×10^{10} and 2.07×10^{10} Jones, for 1, 0.1 and 0.01 V, respectively. In order to estimate the response speed (the time required to increase the photocurrent from 10 to 90% of the peak value or vice versa is defined as the rise time or the fall time, respectively) of the device, one cycle of the photoresponse of the device was plotted in **Figure 5(c)**, from which a rise/fall time of 238.7 and 203.5 s was obtained. This response rate is much slower than other semiconductor based photodetectors. Such a slow response speed is either due to the thermo effect under NIR illumination, or the surface states (e.g. surface dangling bonds, and absorbents) that might act as trapping center, leading to reduced response speed. **Table 1** summarizes the responsivity, on/off ratio, photoconductive gain and detectivity of the present device and other devices based on topological insulators. Remarkably, the main parameters of our photodetector are much better than not only the photodetector based on polycrystalline Bi_2Te_3 film,[23] but also the graphene/Bi_2Te_3 nano-heterojunction device. The relatively good device performance can be ascribed to the location of Dirac point near the Fermi level for the Sb_2Te_3 film.[26, 37] In addition the superior optoelectronic property of Sb_2Te_3 film over that of Bi_2Te_3 is an equally important reason. Such a result suggests the great potential of our topological insulator photodetectors for future optoelectronic devices application.

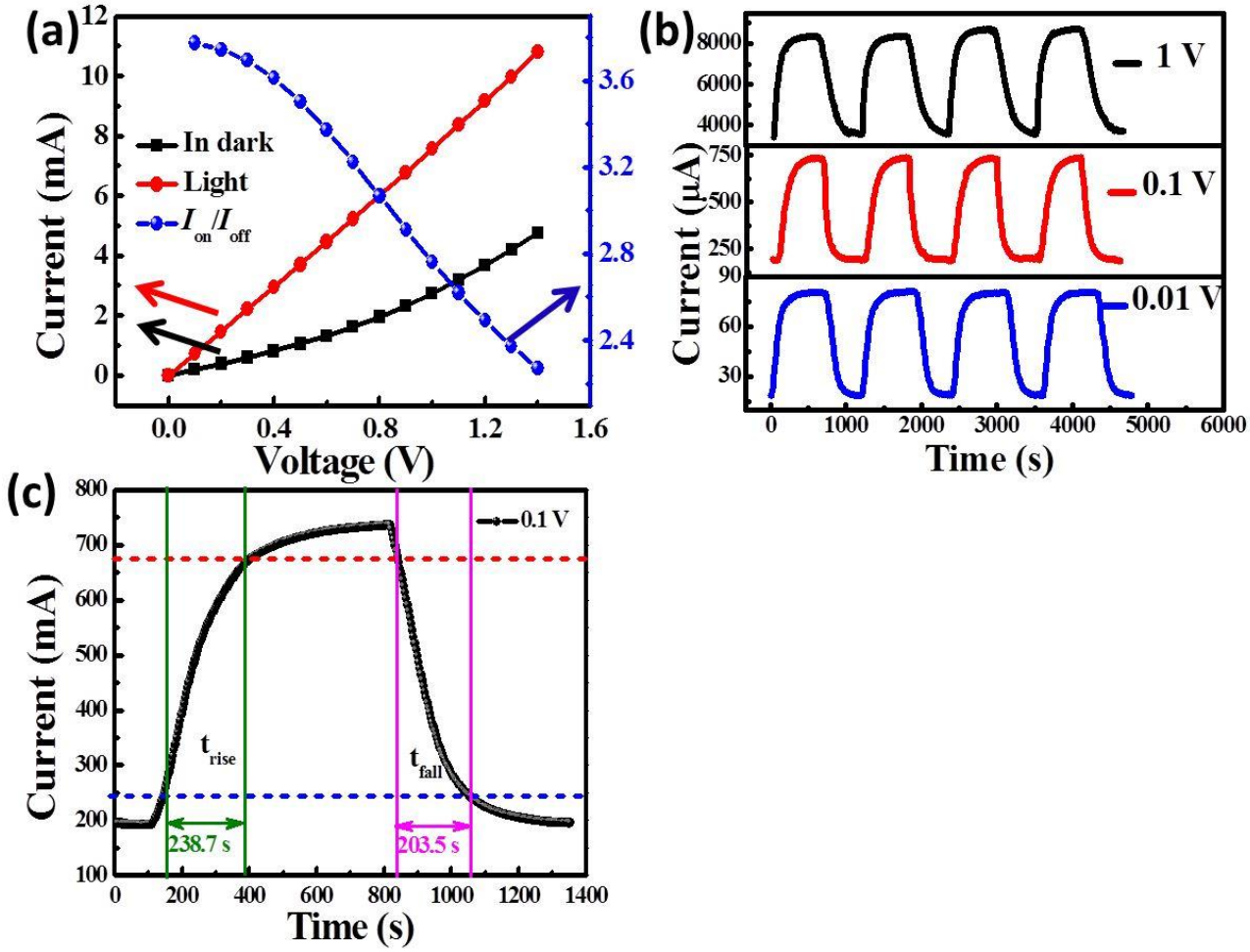

Figure 5 (a) Darkcurrent and photocurrent at temperature of 45 K, blue curves is on/off ratio. (b) Photoresponse of photodetector based on topological insulator Sb_2Te_3 under 45 K at different bias voltage. *V*=0.01 V, 0.1 V, 1 V. (c) One cycle of the photoresponse at the temperature of 45 K, at a bias voltage of 0.1 V.

Table 1 Comparison of the device performance of the present photodetector and other topological insulators based photodetectors.

	Wavelength	***R* (AW^{-1})**	***I*$_{light}$/*I*$_{dark}$**	***G***	***D** (Jones)**	**Reference**
Sb_2Te_3	980 nm	21.7	2.36	27.4	1.22×10^{11}	Our work
Polycrystalline Bi_2Te_3	1064 nm	3.03×10^{-5}	1.0004	3.85×10^{-5}	~	Ref.[23]
Graphene-Bi_2Te_3	980 nm	10	~	11	~	Ref.[24]

The observed high sensitivity can be attributed to unique working mechanism, which is totally different from conventional semiconductor materials based devices. For the present NIR photodetector, when it is irradiated by 980 nm illumination, the resultant photocurrent mainly

consists of two parts: (1) The first contributory factor is associated with the photoconductivity effect of the bulk. Due to the relatively small bandgap of the bulk (~0.26 eV),[6] photocurrent can be easily formed as a result of generation of electron-hole pairs by photons with energy (1.27 eV) much larger than the band-gap. Thus, the bulk contribution may dominate the photoresponse property. (2) The second factor accounting for the photosensitivity is related to the surface states. The pure spin currents which are a net flow of spin without a net flow of charge, are expected to propagate along the surfaces of a topological insulator in equilibrium. When illuminated with polarized light, these pure spin currents can be transformed into a spin-polarized net electrical **(Figure 6)**, which means out of equilibrium for the surface state.[17, 38]

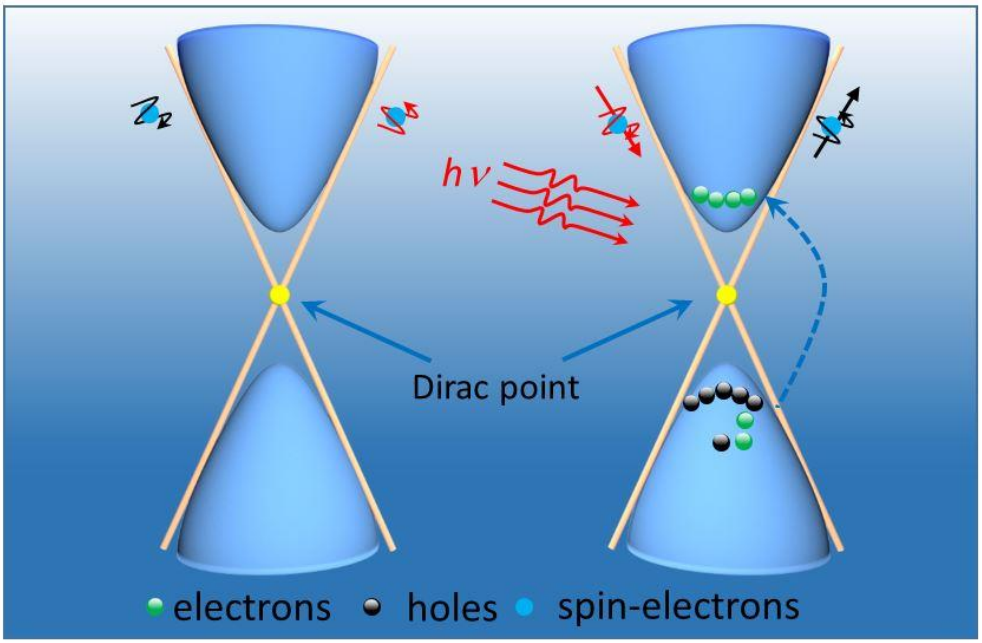

Figure 6 Energy band diagram of the topological insulator photodetector without and with NIR light illumination .

Conclusion

In summary, we report on a NIR photodetector based on topological insulator Sb_2Te_3 thin film which was fabricated by a MBE method. The as-fabricated NIR photodetector exhibits obvious response to the NIR light, with good stability and reproducibility. Further analysis reveals that device

performance of the present device in terms of responsivity, on/off ratio, photoconductive gain and detectivity are much better than other topological insulator materials based devices. This study suggests that the current topological insulator Sb_2Te_3 device will have potential application in future optoelectronic devices.

Experimental Section

Synthesis and characterization of topological insulator Sb_2Te_3 film: The topological insulator Sb_2Te_3 films were grown on sapphire substrate using MBE system at UHV condition. The base pressure was better than 10^{-10} Torr. Both Sb (99.999%) and Te (99.999%) were evaporated from standard Knudsen cells. The growth temperature and Sb/Te flux ratio were kept at 250^{o} C and 2:20, respectively. After synthesis, the microstructure of the Sb_2Te_3 thin film was studied by X-ray diffraction (XRD) and reflected high energy electron diffraction (RHEED). In addition, angle-resolved photoemission spectroscopy (ARPES) analysis was carried out to study the electronic properties of the Sb_2Te_3 film.

Device construction and analysis: Since the topological insulator Sb_2Te_3 film is sensitive to acetone which is usually used to remove photoresist during photolithography process, shadow mask instead of photolithography was employed to define the metal electrode during the fabrication of NIR photodetector. Briefly, copper foil shadow mask was placed on the surface of topological insulator of Sb_2Te_3 thin film, followed by deposition of 25 nm titanium and 35 nm gold film by high vacuum electron beam evaporation. At last, a drop of silver paste was adhered to the Ti/Au electrode. The device characteristics of topological insulator Sb_2Te_3 film were measured using semiconductor characterization system (Keithley 4200-SCS), equipped with an automatic cooling system (CCS-350 Slow temperature cycle refrigeration system). During optoelectronic study, a 980 nm laser was

employed to provide the monochromatic light, which was directly guided to the NIR device.

Reference

1 S. K. Jerng, K. Joo, Y. Kim, S. M. Yoon, J. H. Lee, M. Kim, J. S. Kim, E. Yoon, S. H. Chun, Y. S. Kim, *Nanoscale*, 2013, **5**, 10618-10622.

2 T. Zhang, P. Cheng, X. Chen, J. F. Jia, X. Ma, K. He, L. Wang, H. Zhang, X. Dai, Z. Fang, X. Xie and Q. K. Xue, *Phys. Rev. Lett.*, 2009, **103**, 266803.

3 G. Wang, X. Zhu, J. Wen, X. Chen, K. He, L. Wang, X. Ma, Y. Liu, X. Dai, Z. Fang, J. Jia and Q. Xue, *Nano Res.*, 2010, **3**, 874-880.

4 H. B. Zhang, H. Li, J. M. Shao, S. W. Li, D. H. Bao and G. W. Yang, *ACS Appl. Mater. Interfaces*, 2013, **5**, 11503-11508.

5 Y. Tanaka, Z. Ren, T. Sato, K. Nakayama, S. Souma, T. Takahashi, K. Segawa and Y. Ando, *Nat. Phys.*, 2012, **8**, 800-803.

6 G. Bendt, S. Zastrow, K. Nielsch, P. S. Mandal, J. S. Barriga, O. Rader and S. Schulz, *J. Mater. Chem. A*, 2014, **2**, 8215-8222.

7 X. Chen, X. C. Ma, K. He, J. F. Jia and Q. K. Xue, *Adv. Mater.*, 2011, **23**, 1162-1165.

8 Z. Q. Zeng, T. A. Morgan, D. S. Fan, C. Li, Y. Hirono, X. Hu, Y. F. Zhao, J. S. Lee, J. Wang, Z. M. Wang, S. Q. Yu, M. E. Hawkridge, M. Benamara and G. J. Salamo, *AIP Adv.*, 2013, **3**, 072112

9 M. Z. Hasan and C. L. Kane, *Rev. Mod. Phys.*, 2010, **82**, 3045-3067.

10 J. E. Moore, *Nature*, 2010, **464**, 194-198.

11 J. Wang, A. M. Dasilva, C. Z. Chang, K. He, J. K. Jain, N. Samarth, X. C. Ma, Q. K. Xue, and M. H. W. Chan, *Phys. Rev. B*, 2011, **83**, 245438.

12 Y. Xia, D. Qian, D. Hsieh, L. Wray, A. Pal, H. Lin, A. Bansil, D. Grauer, Y. S. Hor, R. J. Cava

and M. Z. Hasan, *Nat. Phys.*, 2009, **5**, 398-402.

13 Y. H. Wang, D. Hsieh, D. Pilon, L. Fu, D. R. Gardner, Y. S. Lee and N. Gedik, *Phys. Rev. Lett.*, 2011, **107**, 207602.

14 A. Kitaev and J. Preskill, *Phys. Rev. Lett.*, 2006, **96**, 110404.

15 G. P. Collins, *Sci. Adv. Mater.*, 2006, **294**, 56-63.

16 D. Pesin, A. H. Macdonald, *Nat. Mater.*, 2012, **11**, 409-416

17 J. W. McIver, D. Hsieh, H. Steinberg, P. J. Herrero and N. Gedik, *Nat. Nanotechnol.*, 2012, **7**, 96-100.

18 A. Junck, G. Refael and F. von Oppen, *Phys. Rev. B*, 2013, **88**, 075144.

19 C. Zang, X. Qi, L. Ren, G. L. Hao, Y. D. Liu, J. Li and J. X. Zhong, *Appl. Surf. Sci.*, 2014, **316**, 341-347.

20 X. L. Qi and S. C. Zhang, *Rev. Mod. Phys.*, 2011, **83**, 1057-1110.

21 J. M. Shao, H. Li and G. W. Yang, *Nanoscale*, 2014, **6**, 3513-3517.

22 Y. Q. Yu, L. B. Luo, M. Z. Wang, B. Wang, L. H. Zeng, C. Y. Wu, J. S. Jie, J. W. Liu, L. Wang and S. H. Yu, *Nano Res.*, 2015, **8**, 1098-1107.

23 H. B. Zhang, J. D. Yao, J. M. Shao, H. Li, S. W. Li, D. H. Bao, C. X. Wang and G. W. Yang, *Sci. Rep.*, 2014, **4**, 5678.

24 H. Qiao, J. Yuan, Z. Q. Xu, C. Y. Chen, S. H. Lin, Y. S. Wang, J. C. Song, Y. Liu, Q. Khan, H. Y. Hoh, C. X. Pan, S. J. Li and Q. L. Bao, *ACS Nano*, 2015, **9**, 1886-1894.

25 H. B. Zhang, H. L. Yu and G. W. Yang, *Europhys. Lett.*, 2011, **95**, 56002.

26 H. J. Zhang, C. X. Liu, X. L. Qi, X. Dai, Z. Fang and S. C. Zhang, *Nat. Phys.*, 2009, **5**, 438-442.

27 H. W. Liu, H. T. Yuan, N. Fukui, L. Zhang, J. F. Jia, Y. Iwasa, M. W. Chen, T. Hashizume, T. Sakurai and Q. K. Xue, *Cryst. Growth Des.*, 2010, **10**, 4491-4493.

28 M. Z. Wang, W. J. Xie, H. Hu, Y. Q. Yu, C. Y. Wu, L. Wang and L. B. Luo, *Appl. Phys. Lett.*,

2013, **103**, 213111.

29 L. B. Luo, J. J. Chen, M. Z. Wang, H. Hu, C. Y. Wu, Q. Li, L. Wang, J. A. Huang and F. X. Liang, *Adv. Funct. Mater.*, 2014, **24**, 2794-2800.

30 C. Yang, C. J. Barrelet, F. Capasso and C. M. Lieber, *Nano Lett.*, 2006, **6**, 2929-2934.

31 B. Nie, J. G. Hu, L. B. Luo, C. Xie, L. H. Zeng, P. Lv, F. Z. Li, J. S. Jie, M. Feng, C. Y. Wu, Y. Q. Yu and S. H. Yu, *Small*, 2013, **9**, 2872-2879.

32 C. Soci, A. Zhang, B. Xiang, S. A. Dayeh, D. P. R. Aplin, J. Park, X. Y. Bao, Y. H. Lo and D. Wang, *Nano Lett.*, 2007, **7**, 1003-1009.

33 L. B. Luo, F. X. Liang and J. S. Jie, *Nanotechnology*, 2011, **22**. 485701.

34 X. Gong, M. H. Tong, Y. J. Xia, W. Z. Cai, J. S. Moon, Y. Cao, G. Yu, C. L. Shieh, B. Nilsson and A. J. Heeger, *Science*, 2009, **325**, 1665-1667.

35 L. H. Zeng, M. Z. Wang, H. Hu, B. Nie, Y. Q. Yu, C. Y. Wu, L. Wang, J. G. Hu, C. Xie, F. X. Liang and L. B. Luo, *ACS Appl. Mater. Interfaces*, 2013, **5**, 9362-9366.

36 K. K. Manga, J. Z. Wang, M. Lin, J. Zhang, M. Nesladek, V. Nalla, W. Ji and K. P. Loh, *Adv. Mater.*, 2012, **24**, 1697-1702.

37 Y. L. Chen, J. G. Analytis, J. H. Chu, Z. K. Liu, S. K. Mo, X. L. Qi, H. J. Zhang, D. H. Lu, X. Dai, Z. Fang, S. C. Zhang, I. R. Fisher, Z. Hussain and Z. X. Shen, *Science*, 2009, **325**, 178.

38 C. Jozwiak, C. Park, K. Gotlieb, C. Hwang, D. Lee, S. G. Louie, J. D. Denlinger, C. R. Rotundu, R. J. Birgeneau, Z. Hussain, A. Lanzara, *Nat. Phys*. 2013, **9**, 293-298.

Graphical abstract

In this study, we present a photodetector based on topological insulator Sb_2Te_3 thin film, which shows obvious photoresponse to the near infrared light (NIR) at low temperature, with good responsivity, photoconductive gain and detectivity.